

Octahedron-Shaped Linearly Polarized Antenna for Multistandard Services Including RFID and IoT

Ubaid Bashir, Kumud Ranjan Jha, Ghanshyam Mishra, *Student Member, IEEE*,
Ghanshyam Singh, and Satish Kumar Sharma, *Senior Member, IEEE*

Abstract—In this paper, a novel topology of the coplanar waveguide fed truncated octahedron-shaped antenna is proposed. The linearly polarized antenna operates over the triple radio frequency identification technique (RFID) bands of 858–930 MHz, 2.4–2.454 GHz, and 5.725–5.875 GHz at ultra-high frequency (UHF), microwave-, and super high-frequency bands, respectively. In addition, it also supports long-term evolution 4G, TV broadcasting, and 5G bands of the electromagnetic spectrum. The $S_{11} = -10$ dB impedance bandwidth is 294 MHz (697–991 MHz), 120 MHz (2.38–2.5 GHz), 310 MHz (3.07–3.35 GHz), and 310 MHz (5.61–5.92 GHz) in the various bands. The antenna is fabricated on a polyguide substrate of $0.3023\lambda_L \times 0.209\lambda_L \times 0.014\lambda_L$ dimension, where λ_L is the free-space wavelength at the lowest operating frequency. The antenna's S_{11} and the radiation patterns have been measured, and a good agreement between simulated and the measured results has been found. In addition, the proposed antenna is also experimentally verified for the UHF band RFID detection and the global standard for mobile communications 900 band cellular applications. We also propose a system-level schematic to integrate this antenna to other communication standards for the automated RFID applications needed for the Internet of Things.

Index Terms—Internet of Things (IoT), linearly polarized (LP), radio frequency identification technique (RFID), truncated octahedron shape.

I. INTRODUCTION

INTERNET of Things (IoT) are a future generation automated information flow platform, at which, the radio frequency identification technique (RFID) operating in different electromagnetic bands finds the unique applications for the betterment of the humanity [1], [2]. In the recent past, ultrahigh frequency (UHF) band RFID has been attractive to industrial services, goods flow tracking, manufacturing industries, logistic distribution, and the bio-engineering applications [3]–[5]. The another RFID band known as the super high frequency (SHF) RFID performs high-speed tracking, and thus, it can be used for traffic toll collection and the goods management [1], [6]. There are a number of frequency bands assigned to this technology such

Manuscript received June 12, 2016; revised April 8, 2017; accepted April 30, 2017. Date of publication May 17, 2017; date of current version July 1, 2017. (Corresponding author: Kumud Ranjan Jha.)

U. Bashir and K. R. Jha are with Shri Mata Vaishno Devi University, Katra 182320, India (e-mail: 14mmc025@smvdu.ac.in; jhkr@rediffmail.com).

G. Mishra and S. K. Sharma are with the San Diego State University, San Diego, CA 92182 USA (e-mail: ghanshyam1606@gmail.com; ssharma@mail.sdsu.edu).

G. Singh is with the Jaypee University of Information Technology, Solan 173215, India (e-mail: drghanshyam.singh@yahoo.com).

Color versions of one or more of the figures in this paper are available online at <http://ieeexplore.ieee.org>.

Digital Object Identifier 10.1109/TAP.2017.2705097

as UHF band (840–960 MHz), microwave-frequency bands (2.4 Hz–2.48 GHz), and SHF band of 5.72–5.87 GHz whose utilities are governed by the local regulations of a nation.

With the rapid development in IoT, the need to automate the real-time asset and the healthcare management using RFID technique is being experienced and it is an open challenge to the researchers. To make the RFID system automated, there is the need of integrating this technology to the various wireless standards [3]. In any wireless system, the antenna is the RF-front end which plays a crucial role in the system operation and performance. Using an omnidirectional antenna, an RFID automation platform is investigated in [7]. To overcome the uncertainty in the tag antenna polarization, in the past, most of the research focused to develop the linearly polarized (LP) tag and the circular polarized (CP) reader antennas [8]–[13]. However, for the fixed orientation of the tag, the LP antennas can also be used [14] which can save 50% transmitted power in comparison to the CP antenna-based reader when the polarization is matched. Thus, it can optimize the energy use which is much-shouted need of the various IoT networking infrastructures like wireless sensor network and wide area networking [15]. Recently, the use of the LP-based reader antennas in the robotic navigation has been proposed which states that the uncertainty in the tag orientation can be reduced by the transmitted power level tracking and placing the reader antenna on a rotating platform. The LP RFID antennas can also find the suitable applications in the various handheld terminal devices, where the compactness is the main requirement and CP antennas fail to meet this [16]. The most of the LP antennas work in the UHF band and seldom cover other microwave and SHF bands [17]–[25]. However, for the reliable and automated operation, it is necessary to develop a multiband [15] multistandard reader antenna to integrate the RFID system to various networking infrastructure needed for the IoT applications.

In this paper, a novel wideband reader antenna working at three RFID bands 840–960 MHz, 2.40–2.48 GHz, and 5.72–5.87 GHz matched to 50- Ω port characteristic impedance is proposed. In the lower band, the -10 dB impedance bandwidth of the antenna extends over 697–1000 MHz which encompasses various multistandard services like TV broadcasting, global standard for mobile communications (GSM), and long-term evolution (LTE) bands for 4G and 5G communications. To integrate the RFID reader to the IoT infrastructures, a switching/multiplexing schematic using the various communication modules is proposed.

This paper is organized as follows. The antenna topology and its theoretical analysis are discussed in Section II.

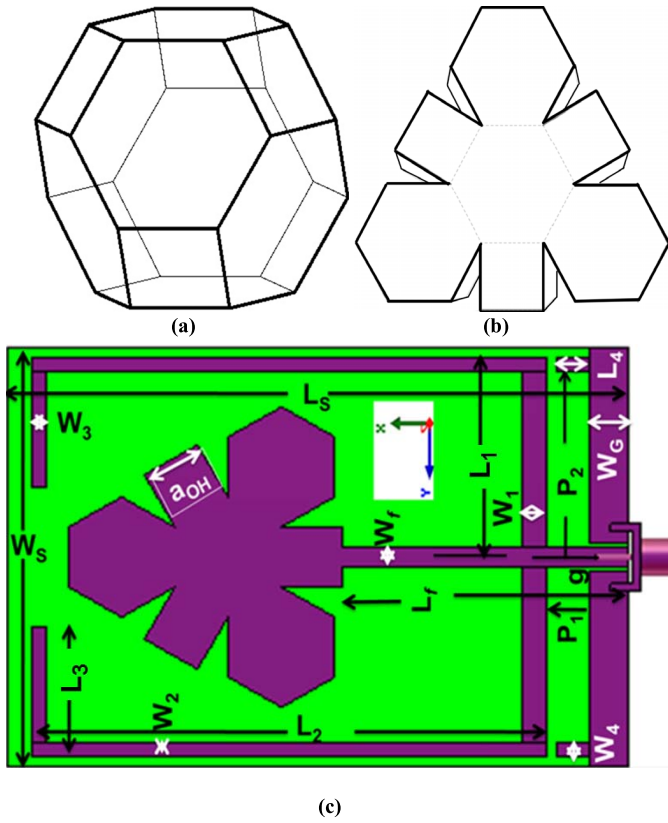


Fig. 1. (a) Truncated octahedron. (b) Half-planar projection. (c) Multiband antenna using this projection.

In Section III, the numerical investigation is presented. In Section IV, the experimental verification of the antenna characteristics is presented. In Section V, the UHF band RFID tag detection is experimentally verified. The application of the antenna in the GSM is also demonstrated. A schematic to integrate this antenna to the various standards is discussed in Section VI. In Section VII, a state-of-the art comparison is presented, and finally, Section VIII concludes the work. The full-wave analysis of the proposed antenna was carried out using time domain solver CST Microwave Studio.

II. ANTENNA TOPOLOGY AND THEORETICAL ANALYSIS

A. Antenna Topology

The proposed multiband antenna designed on a 130 mm × 90 mm × 6.35 mm dimension polyguide substrate ($\epsilon_r = 2.32$ and $\tan \delta = 0.0018$) is shown in Fig. 1. This topology is the planar projection of a truncated octahedron, a kind of the Archimedean solids [26], [27]. The truncated octahedron, its half-planar projection, and the antenna designed using the projection are shown in Fig. 1(a)–(c), respectively. The proposed antenna has a longer perimeter in comparison to many regular polygons which increases the peripheral circulating current path. The longer current path can be exploited to achieve the multiband response with the compact geometry to make the topology suitable for the various wireless communication applications. The proposed structure is a kind of the monopole antenna fed by a coplanar waveguide (CPW). The ground

TABLE I
DESIGN PARAMETERS OF THE PROPOSED ANTENNA

Para meter	Size (mm)						
L_1	39	W_1	5	W_G	9	L_f	130
L_2	110	W_2	3	P_1	8	W_f	90
L_3	24	W_3	3	P_2	39	a_{OH}	12.92
L_4	7	W_4	3	g	1		

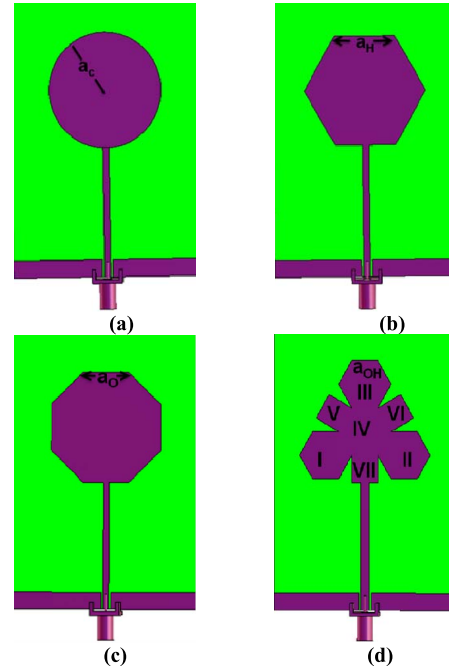


Fig. 2. Different topology of (a) circular, (b) hexagonal, (c) octagonal, and (d) octahedron microstrip patch antenna.

plane and the radiating elements coexist at the same face of the substrate. The various geometrical parameters of the antenna are shown in Table I.

B. Theoretical Analysis

To analyze the resonance behavior of the proposed antenna in Fig. 1, first, we begin with investigating some basic shapes of the planar monopole antennas. These structures are named as microstrip circular patch antenna (MCPA), microstrip hexagonal patch antenna (MHPA), microstrip octagonal patch antenna (MOPA), and microstrip octahedron patch antenna (MOCPA), as shown in Fig. 2(a)–(d), respectively.

We assume that the surface area of the circular (A_C), hexagonal (A_H), octagonal (A_O), and the octahedron (A_{OH}) patches is equal to each other. The geometric areas and perimeters of these patches can be retrieved from a_C , a_H , a_O , and a_{OH} of Fig. 2 with the help of equations given in Table II, where a_C is the radius of the circle and rest are the side lengths of the respective geometry. The truncated octahedron-shaped antenna is made of four hexagonal and three square patches indicated by I–IV and V–VII in Fig. 2(d), respectively. The lengths of the each side of the hexagonal and square shapes are the same,

TABLE II
GEOMETRIC SHAPE RELATION

Geometric Shape	Area	Perimeter
Circle	$A_C = \pi a_c^2$	$P_C = 2\pi a_c$
Hexagonal	$A_H = 1.5a_H^2 \times \sqrt{3}$	$P_H = 6a_H$
Octagonal	$A_O = 2a_O^2 \times (1 + \sqrt{2})$	$P_O = 8a_O$
Octahedron	$A_{OH} = 3a_{OH}^2 + 6a_{OH} \times \sqrt{3}$	$P_{OH} = 24a_{OH}$

and thus, total area of the structure is given by

$$A_{OH} = 3a_{OH}^2 + 6a_{OH} \times \sqrt{3}. \quad (1)$$

The circular patch antenna was explored in [28] and for the same surface area, with the assumption of the effective area equal to the physical area, the MCPA and MHPA are related to each other by the following equation [29]:

$$\pi a_c^2 = \frac{3\sqrt{3}}{2} a_H^2. \quad (2)$$

This equation can also be extended to the other regular shapes without the loss of generality. Accordingly, for the wideband monopole antennas, a relationship between various patch shapes and its lower edge frequency f_L has been investigated in [30] and given by

$$f_L = \frac{7.2}{\{(l + r + p) \times k\}} \text{ GHz}. \quad (3)$$

In (3), l , r , and p are the length, radius, and the feed distance from the ground ($L_f - W_G$) in centimeter, respectively. The k is the effect of the dielectric constant on the lower edge frequency. These parameters can be extracted from different patch shapes as shown in [30]. When the $A_{OH} = A_C = A_O = A_H$, we use the equations shown in Table II to retrieve the geometric parameters of a patch; once the area of any other shape is known. Due to the equal area approximation, it is expected that the resonance frequency of various shaped antennas to be close to each other because the equivalent capacitance in the circuit model is proportional to the area. Based on this, the resonance frequency of octagonal- and octahedron-shaped patches can be retrieved by transforming the patch area to the circular or the hexagonal patch and extracting L , r , and p . However, for the same surface area, the truncated octahedron has the longest perimeter which increases the peripheral current path length.

III. NUMERICAL SIMULATION

The design of an octahedron-shaped multiband antenna begins with selecting $a_{OH} = 12.92$ mm in Fig. 2(d). Using the equivalence area concept, the area and perimeter and the arm length of other topologies are obtained using Table II and the structures are simulated in CST Microwave Studio. The S_{11} response of the various topologies is shown in Fig. 3, and it is observed that the first resonance frequency of the different

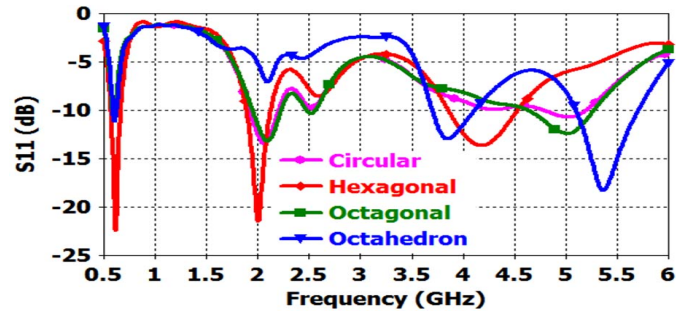


Fig. 3. S_{11} parameter of different shaped antennas.

topologies is in agreement at 0.6 GHz which shows that the concept of the equal area approximation can be extended to the analysis of the proposed topology.

Further, it is noted that the octagonal-shaped antenna closely follows the circular patch due to the close representation of the shape and the minimal truncation deviation in comparison to the other shapes. The hexagonal patch exhibits the excellent impedance matching at various frequencies. The octahedron-shaped antenna shows the improvement in the impedance matching level and the wideband response with respect to others at the higher frequency. However, its impedance matching level is poor ≤ 1 GHz to make suitable for the practical applications below this frequency.

A. Parametric Study

To develop a tri-band antenna operating at three different RFID bands, the proposed topology is parametrically studied. Equation (3) suggests that the ground plane width and the gap distance $p = L_f - W_G$ play a crucial role in controlling the lower operating frequency of the monopole patch antenna, and thus, the effect of varying the W_G on the resonance frequency is shown in Fig. 4.

For the comparison, the effect of this parameter on the circular patch has also been investigated. The variation in W_G does not affect the first resonance frequency and there is a similar up shift in the S_{11} level as shown in the inset. With the increase in W_G , the matching level at 0.6 GHz deteriorates in both the cases. Thus, we conclude that the ground plane has the similar effect on the lower operating band, irrespective of the patch topology and the resonance is mainly being governed by the patch area. We also see that the shorter the width of the ground plane, the better the matching level in these antennas.

B. Bandwidth Enhancement

To enhance the bandwidth of the antenna when operating in the frequency band ≤ 1 GHz and to control the resonance frequencies to make it suitable for RFID applications, the open rectangular loop surrounds the octahedron patch. It consists of three segments indicated by L_1 , L_2 , and L_3 in Fig. 1. The widths of these segments are W_1 , W_2 , and W_3 , respectively. In this section, we explore the effect of the parametric variation and the loading effect of these stubs on the operating bandwidth.

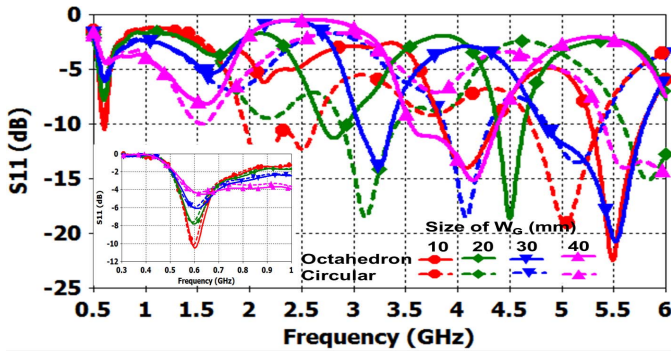


Fig. 4. Effect of the width of the ground plane on the operating bandwidth.

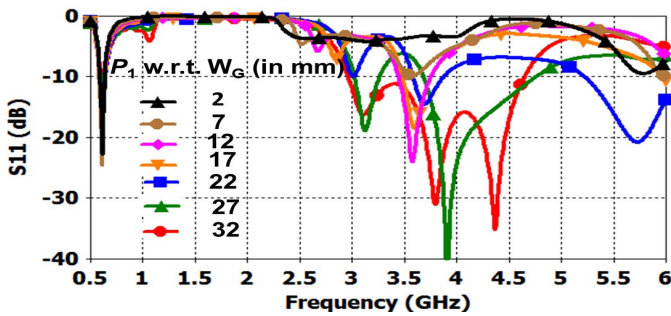


Fig. 5. Effect of the rectangular stub position L_1 on the matching level.

1) *Effect of L_1 Loading*: First of all, $L_1 \times W_1 = 40 \text{ mm} \times 5 \text{ mm}$ rectangular stub, as shown in Fig. 1, is placed on the feed line and its place P_1 , with respect to, the ground plane is varied. When the stub is placed on the feed line as shown in Fig. 1, it improves the matching level in the lower operating frequency band near 600 MHz which is clear from the comparison of Figs. 4 and 5. There is an insignificant effect of the variation in the position of P_1 at the matching level around this frequency. However, it affects in the upper band and by moving away the stub from the ground plane close to the patch ($P_1 = 32 \text{ mm}$), we notice the wideband response in 3–4.6 GHz band. However, an SHF RFID band is still not covered by the antenna.

2) *Effect of the L_2 Stub on the Bandwidth*: To enlarge the operating bandwidth below 1 GHz, two stubs of dimension $L_2 \times W_2$ are now added to the existing first stub L_1 , as shown in Fig. 1. The width W_2 is fixed to 3 mm and length is varied. In Fig. 6, it is noted that with the increase in the length, the impedance bandwidth near 1 GHz improves and for $L_2 \geq 60 \text{ mm}$, the antenna covers the UHF RFID band for the different regulatory due to the lowering of the loaded quality factor of the antenna in this band. However, other two RFID bands are not achieved by the variation in the L_2 even up to 110 mm.

3) *Effect of L_3 on the Convergence of Resonance Frequency*: To precisely control the lower band operation, another two stubs of the dimensions $L_3 \times W_3$ are added to existing L_1 and L_2 as shown in the proposed topology of Fig. 1 and its effect on the impedance bandwidth in Fig. 7. With respect to Fig. 6, the loading of the stub of the length L_3 while $W_3 = 3 \text{ mm}$, marginally increases the -10 dB impedance

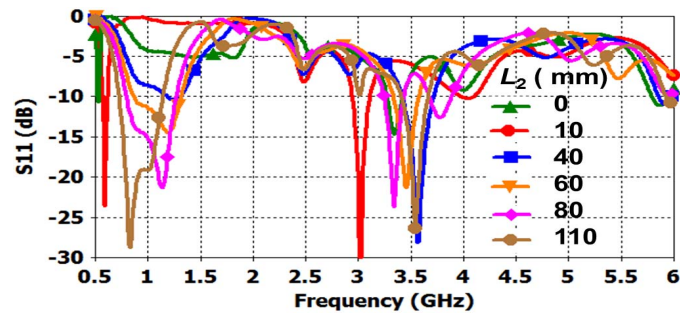


Fig. 6. Effect of the variation of the second stub on the bandwidth.

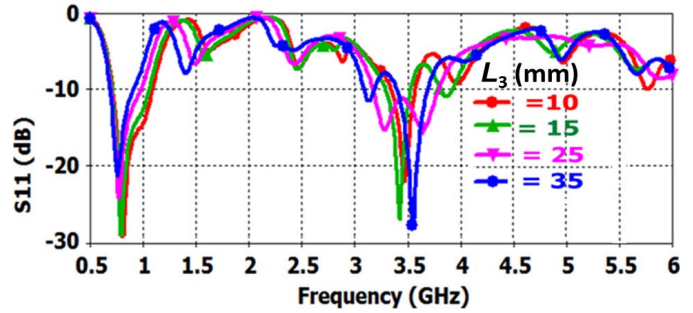


Fig. 7. Effect of the variation in L_3 on impedance matching performance.

bandwidth in the lower band extending from 690 MHz–1 GHz which can cover the various communication bands in addition to the UHF RFID band. However, the effect of the increase in the length inversely controls the bandwidth. When the L_3 has the longer length, due to the coupling with patch and other side stub, the bandwidth reduces and thus we have a tradeoff between the stub size and the bandwidth. The variation in L_3 also shows the convergence of resonance frequencies near 3.5 GHz.

C. Modification in the Ground Plane

In the monopole antennas, the ground plane’s shape and the size play an important role in controlling the impedance bandwidth and the resonance frequencies [31], [32]. Thus, two rectangular stubs of dimension $L_4 \times W_4 = 7 \text{ mm} \times 3 \text{ mm}$ are added to the ground plane as shown in Fig. 1 whose place P_2 governs the upper resonating bands. These stubs do not affect the lower operating band, as shown in Fig. 8. However, above 2 GHz, it helps in getting a number of operating bands. When P_2 is large ($P_2 = 40 \text{ mm}$), due to the coupling between the L_4 and the L_1 improves the impedance matching of the antenna near 2.45 and 5.8 GHz. Three RFID bands obtained are shown as I, II, and IV in Fig. 8. Due to the operation of the truncated octahedron in the higher order modes, a 3.7–4 GHz band is also noted in Fig. 3, which further shifts down due to the external loading of L_3 as discussed in Fig. 7. Further, loading of L_4 also causes a small down shift and thus, an extra 310-MHz bandwidth near center frequency of 3.26 GHz is obtained and this band is marked by III in Fig. 8. The optimized parameters of these stubs are shown in Table III.

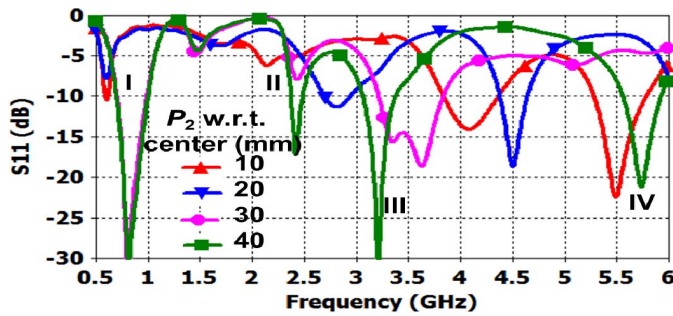


Fig. 8. Effect of the ground plane modification on the impedance matching performance.

TABLE III
OPTIMIZED PARAMETERS OF THE ANTENNA

Parameter	Size (mm)						
L_1	40	W_1	5	W_G	8	L_f	130
L_2	108	W_2	3	P_1	8	W_f	90
L_3	25	W_3	3	P_2	40	a_{OH}	12.9
L_4	8	W_4	3	g	1		

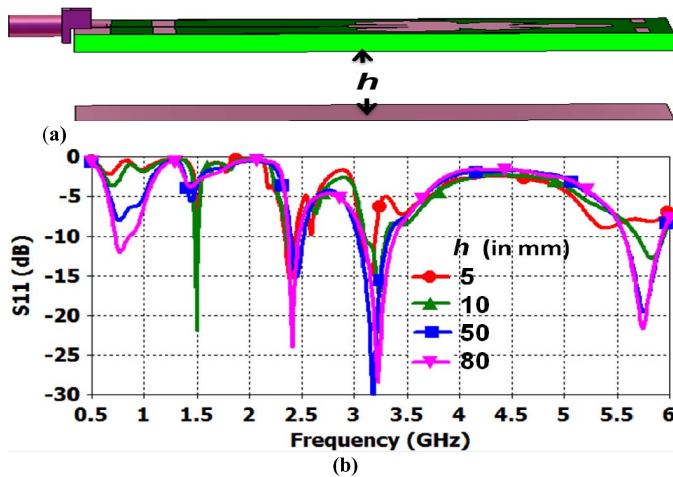


Fig. 9. (a) Position of and (b) its effect on the impedance matching performance.

D. Effect of the Surrounding Metal on the Antenna Operating Band

The proposed antenna is a CPW-fed monopole antenna with the bidirectional detection ability. When a conductor is placed near the antenna, the behavioral change is expected and thus, we study the effect of a substrate size conductor placed near the antenna. We place the conductor at a distance h from the bottom surface of the antenna as shown in Fig. 9(a) and see its effect on the impedance bandwidth in Fig. 9(b).

Fig. 9 shows when $h = 5$ mm, which resembles a kind of the grounded microstrip antenna, the structure resonates at 2.4 and 3.26 GHz. With the increase in the separation to 10 mm, we get all except the band below 1 GHz. When $h = 80$ mm, the lower band is also visible and interestingly, it is found near Fraunhofer boundary of the antenna (79 mm at 700 MHz). The analysis reveals 1) that any metallic object

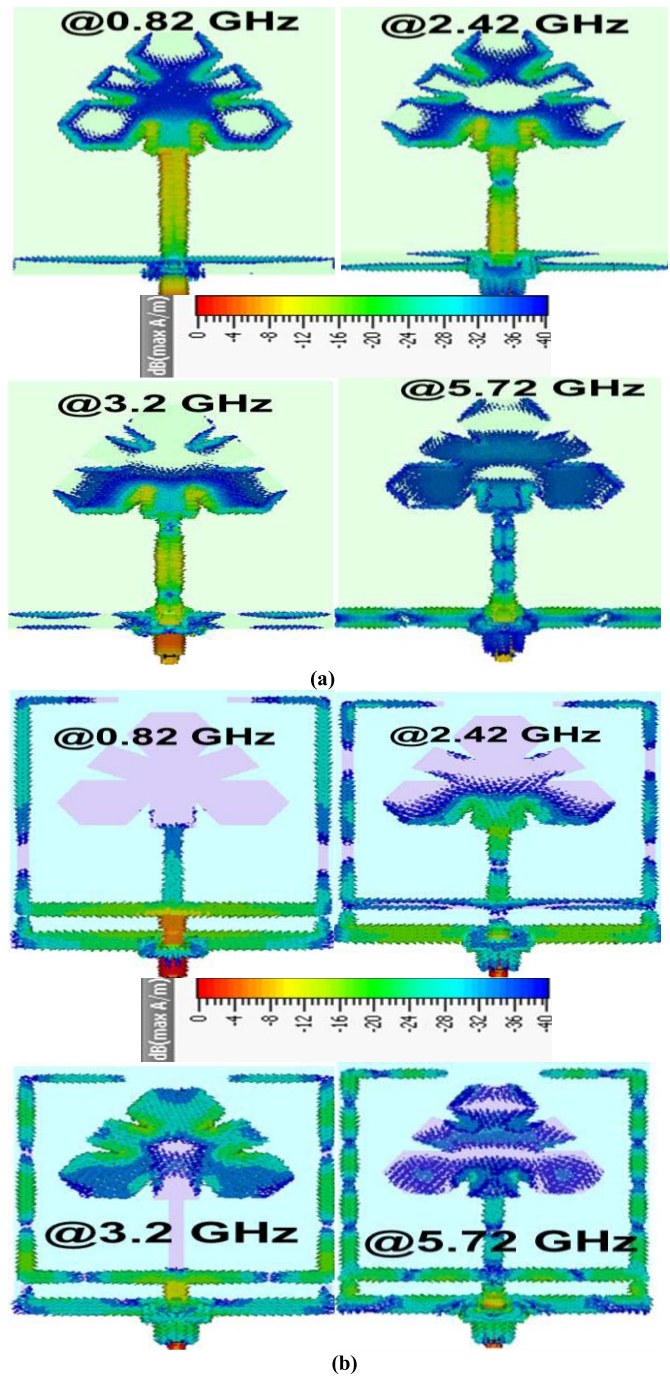


Fig. 10. Surface current density on (a) without loading and (b) with loading on the octahedron patch.

of the ground plane size placed in the far-field region does not affect the multiband band operation and 2) the UHF RFID tag attached on any metallic body can also be detected in this region.

E. Surface Current Distribution

To understand the effect of the various stubs and the ground plane modification on the MOCPA, the surface current density on the antenna surface with and without the external loading

at 0.82, 2.42, 3.2, and 5.72 GHz is shown in Fig. 10(a) and (b), respectively.

When the patch is unloaded, at 0.82 GHz, the surface current is flowing at the perimeter of the antenna and the middle hexagonal patch also takes a part in the radiation mechanism but the impedance matching is poor. At 2.42 GHz, the surface current on the patch increases and flows outward. Similarly, at 3.2 GHz, the lower half of the patch takes a part in the radiation mechanism and at 5.7 GHz, the current density is low at the upper hexagonal surface and the multiple modes are noticed at different frequencies.

When L_1 – L_4 are added to the antenna as shown in Fig. 1, at the frequencies <1 GHz, the radiation is mainly via the stubs and the ground plane also significantly contributes to the radiation mechanism. At 0.82 GHz, the current minima at the open end of L_3 and the joint of L_1 – L_2 can be noticed and the distance between two nulls is about 130 mm which corresponds to about the guided quarter wavelength at 700 MHz. At 2.42 GHz, the octahedron and the stub both contribute to the radiation and the number of current minima increases on the L_2 stub. With the further increase in the operating frequency to 3.2 and 5.72 GHz, the number of current minima increases on the L_2 stub. It is also observed that as the surface current density on the patch is modified, upper perimeter of the structure contributes to the radiation at 3.2 GHz which is governed by L_3 . However, at 5.7 GHz, the extruded ground plane stubs L_4 and the L_1 – L_3 significantly contribute to the radiation and weaker current density is noticed at the patch. Thus, it is concluded that by loading the antenna with the stubs and modifying the ground plane, the multiresonance behavior can be achieved.

IV. EXPERIMENTAL VERIFICATIONS

A. Fabrication and S_{11} Measurement

The proposed antenna was fabricated in Project Laboratory, Shri Mata Vaishno Devi University (SMVDU), India, and measured using vector network analyzer Anritsu model #37269D at the Antenna and Microwave Laboratory, San Diego State University, San Diego, CA, USA. The fabricated structure and its measurement setup are shown in Fig. 11(a) and (b), respectively. The distance between source antenna and the antenna under test is 1.4 m to enable a far-field radiation pattern measurement. The simulated and measured S_{11} parameter of the structure in the frequency range of 0.5–6 GHz is shown in Fig. 12 where a good agreement between the simulated and measured result is observed. The -10 dB impedance bandwidth of the proposed antenna is 294 MHz (697–991 MHz band), 120 MHz (2.38–2.5 GHz band), 310 MHz (3.07–3.35 GHz band), and 310 MHz (5.61–5.92 GHz band) at different frequency bands, respectively. A minor deviation in the results is due to the fabrication tolerance.

B. 2-D Radiation Pattern

The radiation pattern of the antenna at 800 MHz, 2.42 GHz, 3.26 GHz, and 5.78 GHz was measured in the anechoic chamber [Fig. 11(b)] and the normalized measured 2-D pattern

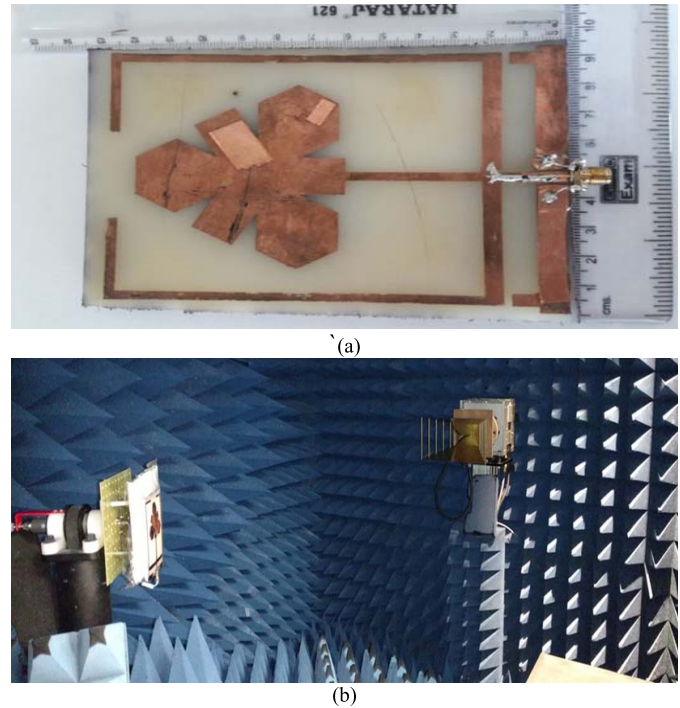


Fig. 11. Photographs of (a) proposed fabricated antenna and (b) measurement setup for the radiation pattern in anechoic chamber.

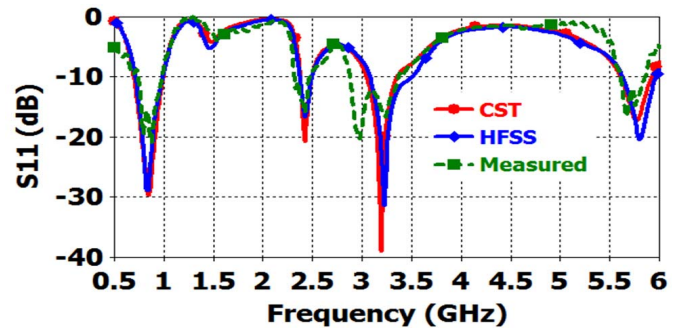


Fig. 12. Simulated and measured S_{11} parameter of the proposed antenna.

along with the simulated ones is shown in Fig. 13(a)–(d), respectively. The cross-polar components in measured results are higher than the simulated ones which are attributed by the small ground plane. Higher cross-polarization components can be an advantage in establishing the link with the linear polarized tag antenna which generally also has higher cross-polarization levels.

C. Peak Realized Gain Over the Frequency Band

The peak realized gain over the frequency is shown in Fig. 14. Due to the nonavailability of the gain table for the Satimo SH800 broadband horn as a reference antenna below 800 MHz, the peak realized gain is only shown in the 0.8–6 GHz range. The measured peak realized gain is extracted from the angular measurement of the 3-D pattern at the interval of 22.5° in the ϕ -plane. The simulated and measured results are in good agreement over the frequency band of interest.

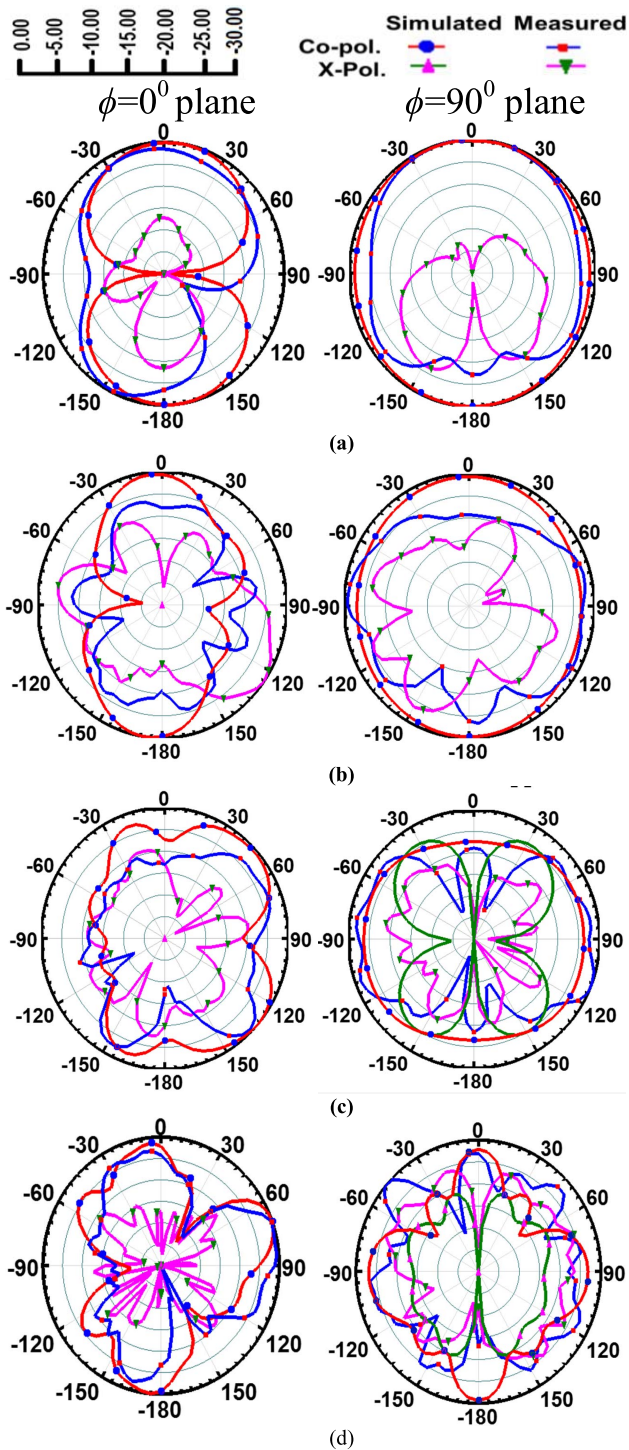


Fig. 13. Normalized simulated and measured radiation pattern at (a) 800 MHz, (b) 2.42 GHz, (c) 3.26 GHz, and (d) 5.78 GHz.

D. 3-D Radiation Pattern

Fig. 15(a)–(d) shows the measured normalized 3-D radiation pattern at 800 MHz, 2.42 GHz, 3.26 GHz, and 5.78 GHz, respectively. To locate the null positions which may be a limiting factor in the RFID applications, the 3-D pattern was measured at the interval of 22.5° in the ϕ -plane. The results show the nulls along the y -axis of the antenna where the RFID detection range may get affected. However, radiation pattern

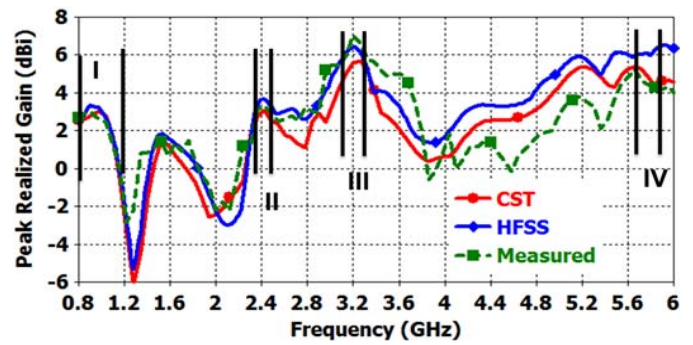


Fig. 14. Simulated and measured peak realized gain over the frequency.

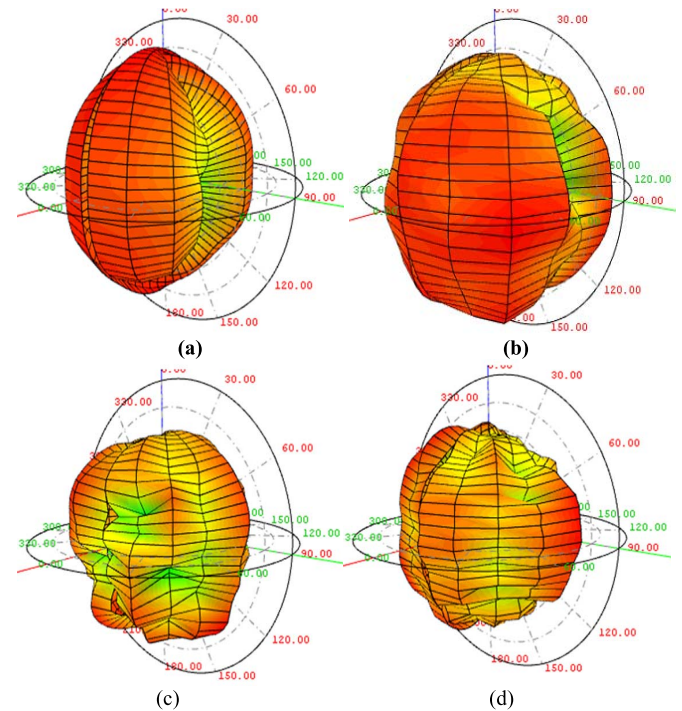
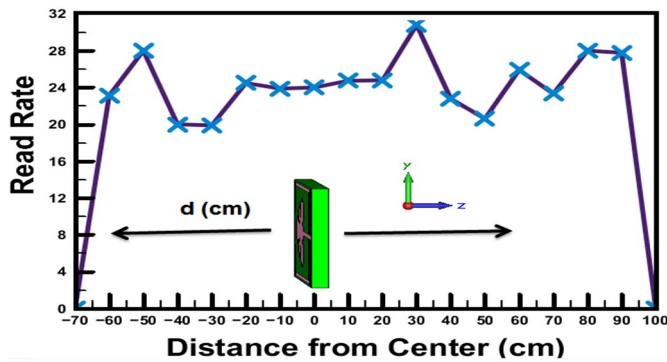


Fig. 15. Measured normalized 3-D radiation pattern at (a) 800 MHz, (b) 2.42 GHz, (c) 3.26 GHz, and (d) 5.78 GHz, respectively.

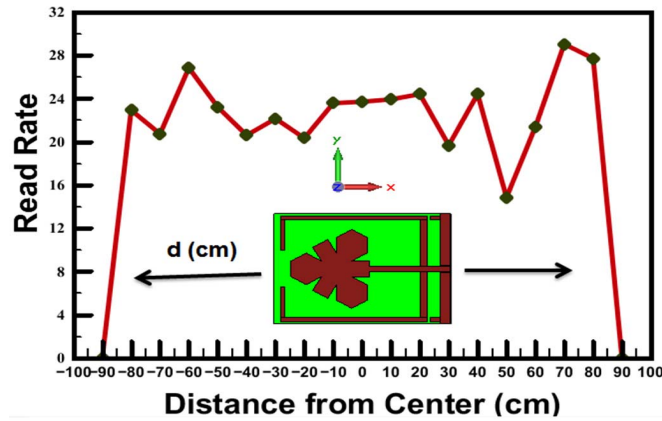


Fig. 16. RFID read range measurement setup.

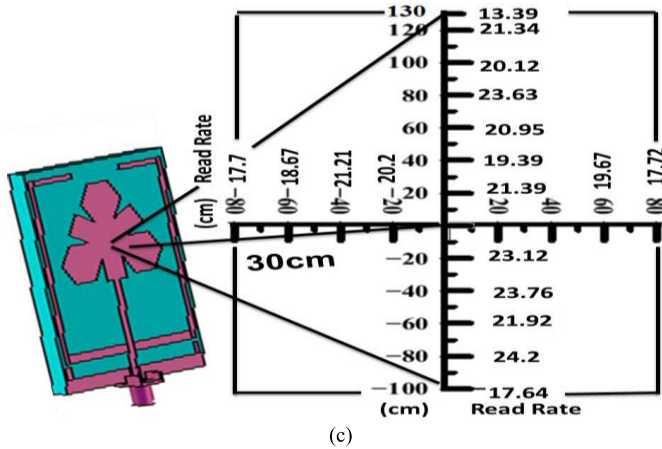
is acceptable along the z - and x -axes (see Fig. 1) for the RFID as well as multistandard services. In addition, due to the small co-planar ground plane, the bidirectional RFID tag detection and communication are possible.



(a)



(b)



(c)

Fig. 17. RFID read range. (a) Perpendicular. (b) Vertical. (c) Coverage in vertical plane.

V. UHF BAND AND GSM SERVICE EXPERIMENTAL RESULTS

A. UHF RFID Tag Detection

In the UHF band, the proposed antenna was used to detect the electronic product code generation 2 RFID tag operating in 860–960 MHz band using a low-cost, low-power AS3992 RFID Reader Module of Austrian Microsystems at SMVDU. The profile of the reader was set as per the USA Standard [33]. The measurement setup is shown in Fig. 16. The measured read count/second at various distances in the different planes is shown in Fig. 17(a)–(c), respectively. The minimum threshold level of the detection, the output power of



Fig. 18. Antenna with the GSM module.

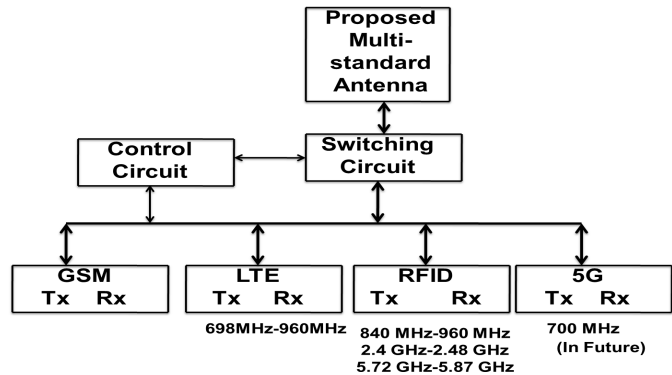


Fig. 19. Proposed schematic for RFID integration.

the transmitter, and the inventory latency period are -40 dBm, 14 dBm, and 10 ms, respectively. The read range was measured in the indoor environment. In all the measurements, tag was placed on the plane which was in parallel to that of the proposed antenna.

B. Antenna Interface With GSM Module

To show the utility of the antenna in the multistandard environments, the antenna was interfaced to a quad band GSM module SIM800 [34] in the GSM 900 band, as shown in Fig. 18. A subscriber identification module (SIM) of cellular service provider BSNL was inserted in the SIM jacket and the connection was established to a cell phone having the SIM of the Airtel another cellular service provider in the region and we were able to establish the contact using this antenna.

VI. INTEGRATION OF THE RFID ANTENNA WITH DIFFERENT COMMUNICATION STANDARDS: A PROPOSAL

The S_{11} parameter of the antenna shows a good -10 dB impedance bandwidth of 294, 1220, 310, and 310 MHz at center frequency of 844 MHz, 2.44 GHz, 3.21 GHz, and 5.765 GHz, respectively. The band below 1 GHz is gaining attention for the 4G-LTE/GSM and 5G wireless communications and thus, the antenna can find multiple applications apart from the RFID. Thus, various communication modules can be integrated to the antenna with the help of the switching/multiplexing unit and the RFID operation can be remotely controlled or automated. The schematic of the proposed system is shown in Fig. 19.

TABLE IV
STATE-OF-ART COMPARISON

Ref. No.	Center Frequency (f_c)	-10 dB Impedance BW	Peak Realized Gain (dBi)	Dimensions (mm ³)	No. of Bands
[17]	900 MHz	160MHz	5	107×124×1.6	Single UHF
[18]	915 MHz 2.45GHz 5.8 GHz	26 MHz 83MHz 150MHz	3.45 2.9 2.55	42×48×0.5	Tri-band
[19]	915 MHz 2.45 GHz 5.8 GHz	170 MHz 900 MHz 1.66 GHz	1.2 2.8 1.0	118×40×1.6	Tri-band
[20]	915 MHz 2.45 GHz 5.8 GHz	50 MHz 310 MHz 1.21 GHz	4.203 2.8 2.46	104×45×6.1	Tri Band
[21]	990MHz	180 MHz	6.5	100×80×1.6	Single
[23]	869.5 MHz	9 MHz	4.0	84×174×3.175	Single UHF
[24]	902MHz 2.4 GHz	202 MHz 120 MHz	3.0 8	160×74×0.8	Double
[25]	930MHz 2.34 GHz 5.94 GHz	260 MHz 370 MHz 880 MHz	2.1 3.98 0.557	97×42×1.6	Tri Band
Proposed	848MHz 2.42 GHz 3.26 GHz 5.78 GHz	303 MHz, 120 MHz, 310 MHz, 310 MHz	2.76 3.29 5.96 5.5	130×90×6.15	Quad-band including Universal UHF, Microwave, SHF RFID, 4G LTE-A, 5G Proposed), TV Broadcasting bands)

VII. STATE-OF-ART COMPARISON

The state-of-art comparison to various LP RFID reader antennas is shown in Table IV.

The state-of-art comparison shows that in addition to the three RFID bands, the proposed antenna has the highest -10 dB impedance bandwidth below 1 GHz which is the precious spectrum for the future wireless communications including the RFID.

VIII. CONCLUSION

A novel topology of a multiband LP RFID reader antenna is proposed. The antenna covers entire UHF RFID band of 840–960 MHz, 2.4-GHz microwave band, and 5.77-GHz SHF band. In addition, it also covers TV bands (697–884 MHz) and GSM bands with -10 dB impedance matching level. The measured S_{11} of the antenna is in good agreement to the simulated result. Both 2-D and 3-D radiation patterns of the proposed antennas are experimentally verified. Additionally, RFID read range is verified using a commercial RFID reader system. The schematic of integrating this antenna to various communication standards is also proposed which can lead toward the automation of the RFID systems for IoT. However, due to the linear polarization, it would be required to know the tag orientation to enhance the reliability.

ACKNOWLEDGMENT

U. Bashir would like to thank B. Singh from the STA Project Laboratory and the Microwave Research Group at SMVDU for the kind support.

REFERENCES

- [1] D. Paret, *RFID at Ultra and Super High Frequencies Theory and Application*. Hoboken, NJ, USA, Wiley, 2009.
- [2] I. Stojmenovic, "Machine-to-machine communications with in-network data aggregation, processing, and actuation for large-scale cyber-physical systems," *IEEE Internet Things J.*, vol. 1, no. 2, pp. 122–128, Apr. 2014.
- [3] S. Amendola, R. Lodato, S. Manzari, C. Occhiuzzi, and G. Marrocco, "RFID technology for IoT-based personal healthcare in smart spaces," *IEEE Internet Things J.*, vol. 1, no. 2, pp. 144–152, Apr. 2014.
- [4] J. H. Lu and S. F. Wang, "Planar broadband circularly polarized antenna with square slot for UHF RFID reader," *IEEE Trans. Antennas Propag.*, vol. 61, no. 1, pp. 45–53, Jan. 2013.
- [5] L. Toivanen, M. Heino, A. Oksman, A. Vienamo, J. Holopainen, and V. Viikari, "RFID-based book finder," *IEEE Antennas Propag. Mag.*, vol. 58, no. 3, pp. 72–80, Mar. 2016.
- [6] C. Varadhan, J. K. Pakkathillam, M. Kanagasabai, R. Sivasamy, R. Natarajan, and S. K. Palaniswamy, "Triband antenna structures for RFID systems deploying fractal geometry," *IEEE Antennas Wireless Propag. Lett.*, vol. 12, pp. 437–440, Apr. 2013.
- [7] M. Bolic, M. Rostamian, and P. Djuric, "Proximity detection with RFID: A step toward the Internet of Things," *IEEE Pervasive Comput.*, vol. 14, no. 2, pp. 70–76, Feb. 2015.
- [8] J. Virkki *et al.*, "Reliability of washable wearable screen printed UHF RFID tags," *Microelectron. Rel.*, vol. 54, no. 4, pp. 840–846, 2014.
- [9] M. S. Khan, M. Islam, and H. Deng, "Design of a reconfigurable RFID sensing tag as a generic sensing platform toward the future Internet of Things," *IEEE Internet Things J.*, vol. 1, no. 4, pp. 300–310, Apr. 2014.
- [10] C. Raviteja, C. Varadhan, M. Kanagasabai, A. K. Sarma, and S. Velan, "A fractal-based circularly polarized UHF RFID reader antenna," *IEEE Antennas Wireless Propag. Lett.*, vol. 13, pp. 499–502, May 2014.
- [11] R. Cao and S. Yu, "Wideband compact CPW-fed circularly polarized antenna for universal UHF RFID reader," *IEEE Trans. Antennas Propag.*, vol. 63, no. 9, pp. 4148–4151, Sep. 2015.
- [12] E. Mireles and S. Sharma, "A novel wideband circularly polarized antenna for worldwide UHF band RFID reader applications," *Progr. Electromagn. Res. B*, vol. 42, pp. 23–44, Sep. 2012.
- [13] X. Liu, Y. Liu, and M. M. Tentzeris, "A novel circularly polarized antenna with coin-shaped patches and a ring-shaped strip for worldwide UHF RFID applications," *IEEE Antennas Wireless Propag. Lett.*, vol. 14, pp. 707–710, Sep. 2015.
- [14] R. Drori, accessed on Jun. 7, 2016. [Online]. Available: http://www.mtiwe.com/_Uploads/.../Selecting_RFID_Antennas-White
- [15] S. Li, L. Xu, and S. Zhao, "The Internet of Things: A survey," *Inf. Syst. Frontiers*, vol. 17, no. 2, pp. 243–259, 2015.
- [16] L. Catarinucci, S. Tedesco, and L. Tarricone, "Customized ultra high frequency radio frequency identification tags and reader antennas enabling reliable mobile robot navigation," *IEEE Sensors J.*, vol. 13, no. 2, pp. 783–791, Feb. 2013.
- [17] H.-T. Hsu and T.-J. Huang, "A koch-shaped log-periodic dipole array (LPDA) antenna for universal ultra-high-frequency (UHF) radio frequency identification (RFID) handheld reader," *IEEE Trans. Antennas Propag.*, vol. 61, no. 9, pp. 4852–4856, Sep. 2013.
- [18] A. M. Montaser, "Reconfigurable antenna for RFID reader and notched UWB applications using DTO algorithm," *Progr. Electromagn. Res. C*, vol. 47, pp. 65–74, Sep. 2014.
- [19] A. T. Mobashsher, M. T. Islam, and N. Misran, "Triple band RFID reader antenna for handheld applications," *Microw. Opt. Technol. Lett.*, vol. 53, no. 7, pp. 1629–1632, 2011.
- [20] A. M. Montaser, H. A. Elmikati, and K. R. Mahmoud, "Tri-band slotted bow-tie antenna design for RFID reader using hybrid CFO-NM algorithm," in *Proc. 29th Nat. Radio Sci. Conf.*, Cario, Egypt, Apr. 2012, pp. 82–89.
- [21] M. R. Zaman, R. Azim, N. Misran, M. F. Asillam, and T. Islam, "Development of a semielliptical partial ground plane antenna for RFID and GSM-900," *Int. J. Antennas Propag.*, vol. 2014, 7 pages, 2014, Art. no. 693412.
- [22] Y. Wang, A. J. Pretorius, and A. M. Abbosh, "Low-profile antenna with elevated toroid-shaped radiation for on-road reader of RFID-enabled vehicle registration plate," *IEEE Trans. Antennas Propag.*, vol. 64, no. 4, pp. 1520–1525, Apr. 2016.
- [23] B. Shrestha, A. Elsherbeni, and L. Ukkonen, "UHF RFID reader antenna for near-field and far-field operations," *IEEE Antennas Wireless Propag. Lett.*, vol. 10, pp. 1274–1277, Sep. 2011.
- [24] H. Hsu and T. Huang, "A 1×2 dual-band antenna array for radio-frequency identification (RFID) handheld reader applications," *IEEE Trans. Antennas Propag.*, vol. 62, no. 10, pp. 5260–5267, Oct. 2014.

- [25] L. You, K. Zhou, X.-F. Zhang, and C.-S. Tian, "A novel triple band antenna for RFID handheld reader," in *Proc. Wireless Commun. Netw. Mobile Comput.*, Beijing, China, Sep. 2014, pp. 615–618.
- [26] *Archimedean Solid—From Wolfram MathWorld Mathworld. Wolfram*, accessed on Jun. 1, 2016. [Online]. Available: <http://mathworld.wolfram.com/ArchimedeaneSolid.html>
- [27] (2016). Accessed on Dec. 5, 2016. [Online]. Available: <http://mathcs.wilkes.edu/~rpryor/mth343/solidGeometry.pdf>
- [28] C. A. Balanis, *Antenna Theory and Design*. Hoboken, NJ, USA: Wiley, 2005.
- [29] N. Kushwaha and R. Kumar, "Design of slotted ground hexagonal microstrip patch antenna and gain improvement with FSS screen," *Progr. Electromagn. Res. B*, vol. 51, pp. 177–199, Sep. 2013.
- [30] K. P. Ray, "Design aspects of printed monopole antennas for ultra-wide band applications," *Int. J. Antennas Propag.*, vol. 2008, 8 pages, 2008, Art. no. 713858.
- [31] H. N. Tripathi, S. Shukla, R. Aggarwal, K. R. Jha, and N. Tripathi, "Effects of planar ground plane structure on elliptical-shaped patch antenna for wireless UWB applications," in *Proc. Students Conf. Eng. Syst.*, Allahabad, India, May 2014, pp. 1–4.
- [32] K. R. Jha, G. Mishra, and S. K. Sharma, "An octahedron shaped planar antenna for IoT applications," in *Proc. IEEE Int. Symp. Antennas Propag.*, San Diego, CA, USA, Jul. 2017, pp. 1–2.
- [33] (2016). *AS3992—UHF RFID Single Chip Reader with Dense Reader Mode-AMS*, *Ams. Com*, accessed on Dec. 2, 2016. [Online]. Available: <http://ams.com/eng/Products/Wireless-Connectivity/Readers/AS3992>
- [34] (2016). *SIM800 Simcomm2m. Com*, accessed on Dec. 2, 2016. [Online]. Available: <http://simcomm2m.com/En/module/detail.aspx?id=138>



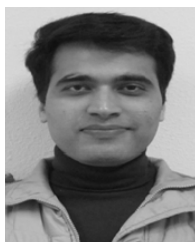
Ubaid Bashir was born in Srinagar, India. He received the B.E. degree in electronics and communication engineering from the University of Jammu, Jammu, India, in 2012, and the M.Tech. degree in electronics and communication engineering from Shri Mata Vaishno Devi University, Katra, India, in 2016. He qualified GATE examination in 2014.



Kumud Ranjan Jha received the bachelor's and master's degrees in electronics and communication engineering from The Institution of Engineers (India) and Birla Institute of Technology, Ranchi, Jharkhand, India in 1999 and 2007, respectively, and the Ph.D. degree from the Jaypee University of Information Technology, Solan, India, in 2012.

He has served at Indian Air Force. In 2007, he joined Shri Mata Vaishno Devi University, Katra, India, as an Assistant Professor, where he is currently an Associate Professor. In 2012, he was

awarded the Raman Fellowship from the University Grant Commission, Government of India, for the Post-Doctoral Study in USA. He is currently a Post-Doctoral Fellow with San Diego State University, San Diego, CA, USA. He has authored more than 60 peer-reviewed research articles in the international journals and conferences of repute, and co-authored a book *Terahertz Planar Antennas for Next Generation Communication*. His current research interests include microwave/RF passive/active component design and terahertz electronics for the future wireless communication.



Ghanshyam Mishra (S'16) received the M.Tech. degree in RF and microwave engineering from IIT Kharagpur, Kharagpur, India, in 2013. He is currently pursuing the Ph.D. degree with San Diego State University, San Diego, CA, USA.

His current research interests include millimeter-wave high-gain beam steering antennas, feed horn and reflector antennas, and wideband and wide scanning phased arrays.



Ghanshyam Singh received the Ph.D. degree in electronics engineering from IIT, Banaras Hindu University, Varanasi, India, in 2000.

He was a Research Scientist with the Central Electronics Engineering Research Institute, Pilani, India, and with the Institute for Plasma Research, Gandhinagar, India. He was with the Nirma University of Science and Technology, Ahmedabad, India. He was a Visiting Researcher at the Seoul National University, Seoul, South Korea. He is currently a Professor with the Department of Electronics and

Communication Engineering, Jaypee University of Information Technology, Solan, India. He has more than 14 years of teaching and research experience in the area of electromagnetic/microwave engineering, wireless communication, and nanophotonics. He has supervised various Ph.D. and M.Tech. theses. He has authored or co-authored more than 200 scientific articles of the refereed journal and international conferences, and authored four books published by Springer. His current research interests include RF/microwave engineering, millimeter-/terahertz-wave antennas and its applications in communication and imaging, next-generation communication systems (OFDM and cognitive radio), and nanophotonics.

Dr. Singh served as a reviewer for several reputed journals and conferences.



Satish Kumar Sharma (SM'04) received the B.Tech. degree in electronics engineering from the Kamla Nehru Institute of Technology, Sultanpur, India, in 1991, and the Ph.D. degree in electronics engineering from IIT, Banaras Hindu University, Varanasi, India, in 1997.

From 1999 to 2001, he was a Post-Doctoral Fellow with the Department of Electrical and Computer Engineering, University of Manitoba, Winnipeg, MB, Canada, where he was also a Research Associate, from 2001 to 2006. From 2001 to 2006, he was

a Senior Antenna Engineer with InfoMagnetics Technologies Corporation, Winnipeg. In 2006, he joined the Department of Electrical and Computer Engineering, San Diego State University (SDSU), San Diego, CA, USA, as an Assistant Professor, where he has developed an Antenna Laboratory, teaches courses in applied electromagnetics, and advises M.S. and Ph.D. graduate students and Post-Doctoral Fellows. He is currently a Professor and the Director of the Antenna and Microwave Laboratory, SDSU. He has authored or co-authored more than 185 research papers published in the refereed international journals and conferences, and co-edited three volumes of *Handbook of Reflector Antennas and Feed Systems*, Volume I: Theory and Design of Reflectors, Volume II: Feed Systems, and Volume III: Applications of Reflectors (Artech House, USA), which also has several co-authored chapter contributions by him. He holds one U.S. and one Canadian patents. His current research interests include the millimeter-wave antennas, beam steering antennas, massive MIMO antennas, 5G communication antennas, beamforming networks, antennas for Internet of Things, microstrip antennas, ultra-wideband, multiband and broadband antennas, reconfigurable and frequency agile antennas, feeds for reflector antennas, waveguide horns and polarizers, electrically small antennas, RFID antennas, active antennas, and microwave passive components.

Dr. Sharma is a Full Member of the USNC/URSI, Commission B, Fields and Waves. He was a recipient of the IEEE AP-S Harold A. Wheeler Prize Paper Award in 2015, the National Science Foundation's prestigious faculty early development (CAREER) award in 2009, and the Young Scientist Award of URSI Commission B, Field and Waves, during the URSI Triennial International Symposium on Electromagnetic Theory, Pisa, Italy, in 2004. He was recognized as the Outstanding Associate Editor (AE) of the IEEE TRANSACTION ON ANTENNAS AND PROPAGATION (IEEE TAP) journal in 2014. He was a Chair/Co-Chair of the several student paper contests in different conferences and symposia and served on the subcommittee of the Education Committee for the IEEE Antennas and Propagation Society for the organization of the student paper contests. He has been serving as an AE of the IEEE TAP since 2010 and the IEEE ANTENNAS AND WIRELESS PROPAGATION LETTERS since 2017.